

Replication enhancer elements within the open reading frame of tick-borne encephalitis virus and their evolution within the Flavivirus genus

Article

Published Version

Tuplin, A., Evans, D. J., Buckley, A., Jones, I. M. ORCID: <https://orcid.org/0000-0002-7738-2516>, Gould, E. A. and Gritsun, T. S. (2011) Replication enhancer elements within the open reading frame of tick-borne encephalitis virus and their evolution within the Flavivirus genus. *Nucleic Acids Research*, 39 (16). pp. 7034-7048. ISSN 1362-4962 doi: <https://doi.org/10.1093/nar/gkr237> Available at <https://centaur.reading.ac.uk/20728/>

It is advisable to refer to the publisher's version if you intend to cite from the work. See [Guidance on citing](#).

Published version at: <http://nar.oxfordjournals.org/content/early/2011/05/27/nar.gkr237.full.pdf?keytype=ref&ijkey=UI6dZzMlfQmcV2t>

To link to this article DOI: <http://dx.doi.org/10.1093/nar/gkr237>

Publisher: Oxford University Press

All outputs in CentAUR are protected by Intellectual Property Rights law, including copyright law. Copyright and IPR is retained by the creators or other copyright holders. Terms and conditions for use of this material are defined in the [End User Agreement](#).

www.reading.ac.uk/centaur

CentAUR

Central Archive at the University of Reading

Reading's research outputs online

Replication enhancer elements within the open reading frame of tick-borne encephalitis virus and their evolution within the *Flavivirus* genus

A. Tuplin¹, D. J. Evans¹, A. Buckley², I. M. Jones³, E. A. Gould⁴ and T. S. Gritsun^{3,*}

¹School of Life Sciences, University of Warwick, Coventry, CV4 7AL, ²Cranfield Health, Cranfield University, Cranfield, Bedfordshire MK43 0AL, UK, ³School of Biological Sciences, University of Reading, Whiteknights, Reading, RG6 6AJ, UK and ⁴Unité des Virus Emergents, Faculté de Médecine Timone, 5ème étage Aile Bleu, 27, Bd Jean Moulin, 13385 Marseille, Cedex 05, France

Received February 6, 2011; Revised March 31, 2011; Accepted April 5, 2011

ABSTRACT

We provide experimental evidence of a replication enhancer element (REE) within the capsid gene of tick-borne encephalitis virus (TBEV, genus *Flavivirus*). Thermodynamic and phylogenetic analyses predicted that the REE folds as a long stable stem-loop (designated SL6), conserved among all tick-borne flaviviruses (TBFV). Homologous sequences and potential base pairing were found in the corresponding regions of mosquito-borne flaviviruses, but not in more genetically distant flaviviruses. To investigate the role of SL6, nucleotide substitutions were introduced which changed a conserved hexanucleotide motif, the conformation of the terminal loop and the base-paired dsRNA stacking. Substitutions were made within a TBEV reverse genetic system and recovered mutants were compared for plaque morphology, single-step replication kinetics and cytopathic effect. The greatest phenotypic changes were observed in mutants with a destabilized stem. Point mutations in the conserved hexanucleotide motif of the terminal loop caused moderate virus attenuation. However, all mutants eventually reached the titre of wild-type virus late post-infection. Thus, although not essential for growth in tissue culture, the SL6 REE acts to up-regulate virus replication. We hypothesize that this modulatory role may be important for TBEV survival in nature, where the virus circulates by non-viraemic transmission between infected and non-infected ticks, during co-feeding on local rodents.

INTRODUCTION

Tick-borne encephalitis virus (TBEV) is a human pathogen that causes about 16 000 human cases of tick-borne encephalitis (TBE) across Europe and Asia annually (1–3). Taxonomically, TBEV is a species within the mammalian tick-borne flaviviruses (mTBFV). Together with the seabird tick-borne flavivirus group (sTBFV), they comprise one ecological group of tick-borne flaviviruses (TBFV) within the genus *Flavivirus*, family *Flaviviridae*. Two other ecological groups within the genus *Flavivirus* are the mosquito-borne flaviviruses (MBFV) and flaviviruses with no-known vector (NKV) (4). A fourth group including Kamiti River virus (KRV) (5), cell fusion agent virus (CFAV) (6) and *Culex* flavivirus (CuFV) (7) have been isolated only from mosquitoes with no demonstrated capacity to replicate in mammals and are under consideration by the ICTV Committee for classification as ‘probably arthropod-borne viruses’ (PABV).

Flavivirus virions are ~50-nm particles with a nucleocapsid composed of capsid (C) protein surrounding a positive-sense single-stranded RNA genome of ~11 kb. The capsid is enclosed in a lipid membrane within which the viral membrane (M) and envelope (E) proteins are embedded. The genome encodes a single polyprotein of approximately 3400 amino acids from which the three structural (C, M and E) and seven non-structural (NS1, NS2A, NS2B, NS3, NS4A, NS4B and NS5) proteins are processed by cellular and viral proteases (8).

Flavivirus genome replication involves synthesis of a negative-sense template strand by the RNA-dependent RNA polymerase (RdRp; NS5^{pol}) from which additional genome-sense strands are transcribed. This process is controlled by numerous RNA–RNA and RNA–protein interactions determined by virus RNA sequence motifs and secondary structures, called *cis*-acting replication

*To whom correspondence should be addressed. Tel: +44 0118 378 6368; Fax +44 (0)118 378 6537; Email: t.s.gritsun@reading.ac.uk

elements (CRE), mapped to the 5'- and 3'-untranslated regions (UTR) that flank the single open reading frame (ORF) of the genome (9–15).

The concept of promoter and enhancer function during replication has been introduced recently in relation to the flavivirus CREs (16). The promoter has been identified as a complex of highly conserved interacting RNA structures recruited from the 5'- and 3'-UTR to assemble viral and cellular proteins into a functional RdRp complex. In evolutionary terms, the 3'-UTR of the TBFV group is formed by four conserved long imperfectly repeated sequences (LSRs), genetic remnants of which are revealed in the MBFV, NKV and PABV groups (17). It has been proposed that the 5'-UTR may have evolved from a trans-terminal duplication of the archival flavivirus 3'-UTR (16).

An additional complexity in flavivirus replication is the presence of replication enhancer elements (REEs) in the 3'-UTR that, while not obligatory for replication of laboratory-maintained viruses, are likely essential for virus circulation and transmission in nature (16,18). Engineered deletions or modifications of the REEs enable the recovery of viable viruses that are attenuated as a result of reduced RNA synthesis (10,19–22). The cumulative effect of several REEs enhances the assembly of the RdRp complex and is probably critical to the survival of flaviviruses in nature (23). The REEs identified for MBFV have become an important target for the development of a live attenuated vaccine for dengue virus (24,25).

The relatively compact nature of the flavivirus genome, together with constraints imposed by the need to replicate in vertebrate and invertebrate hosts, means that additional CRE sequences may be present in parts of the genome other than the non-coding regions. Indeed, RNA secondary structures have been predicted within the coding region of several flaviviruses (26–28). Here, using bioinformatic and reverse genetic analysis we demonstrate that the capsid-encoding region of TBEV contains an REE which we designate SL6 (26,27). Phylogenetic evidence suggests that the MBFV group also contains at least a partial SL6-like structure, though it is absent in the NKV or PABV groups. The significance of these findings in the context of flavivirus evolution and adaptation to transmission is discussed.

MATERIALS AND METHODS

Sequence and structural analysis

Genbank accession numbers for sequences from all four groups of flaviviruses (TBFV, MBFV, NKV and PABV) used for *in silico* analysis are listed in [Supplementary Table S1](#). RNA nucleotide sequences were aligned using ClustalX (29) and then edited manually. Nucleotide and dinucleotide scans and analysis of suppression of synonymous site variability (SSSV) were determined by mean pair-wise distance comparison at each codon within the ORF using the Simmonics 1.6 package (<http://www.picornavirus.org/>), as previously described (30). SSSV was calculated only at aligned codon positions

in which over 40% of sequence comparisons were synonymous and averaged over a sliding window of 21 codons; consequently, data point are only produced from codon 11.

RNA secondary structures were predicted using the MFold 3.2 and DINAMelt packages (<http://mfold.bioinfo.rpi.edu/>) with default settings (31,32). Phylogenetically conserved RNA structures were predicted using STRUCTURE_DIST (<http://www.picornavirus.org/>) to analyze connect files generated using hybrid-ss-min from the UNAFold suite of programs (32).

Cells and viruses

Porcine embryo kidney cells (PS) have been used in experiments with TBEV strain Vasilchenko (Vs) and its infectious clone (pGGVs) as described previously (33–35).

Plasmids and site-directed mutagenesis

The construction of the infectious clone pGGVs for Vs virus and methods of mutagenesis have been described (34,36). Briefly, the pGGVs was subcloned into two plasmids; one, pGGVs₆₆₀ contained the first 660 nt of the virus genome and the second pGGVs_{660–10927} included the remainder. Site-directed mutagenesis was accomplished by PCR (details of primers are available on request). Mutated PCR products were cloned into the pGGVs₆₆₀ between MluI and EcoRI sites followed by sequencing.

Recovery of viruses from infectious clone

The recovery of virus from the two plasmids representing the infectious clone has been described previously (34–36). Briefly, plasmid pGGVs₆₆₀ (or mutated derivatives) was digested with PspAI, dephosphorylated with Shrimp Alkaline Phosphatase (SAP; USB) and, after heat-inactivation of SAP, digested with AgeI. Similarly, pGGVs_{660–10927} was digested with NotI, dephosphorylated and then digested with AgeI. The excised linker DNA fragments from pGGVs₆₆₀ and pGGVs_{660–10927} were removed using MicroSpin™ S-400 columns (Pharmacia Biotech) and ligated at the AgeI site generating full-length cDNA which was linearized with SmaI and used as a template for SP6 transcription (34). *In vitro*-synthesized RNA was inoculated intracerebrally into suckling mice to recover the mutant viruses which were not passaged further prior to phenotype evaluation (35). Recovered viruses were amplified by RT-PCR between nucleotides 1–940 (5'-UTR-C-prM region of the TBEV genome) and 10206–10927 (3'-UTR), and sequenced to validate the presence of the introduced mutations and to exclude extraneous mutations at the 5'-UTR and 3'-UTR (36).

Analysis of virus replication cycle and cytopathic effect

For growth curves, monolayers of PS cells in 96-well plates were infected with viruses at a multiplicity of infection (moi) of 1 PFU/cell, in quadruplicates. The inoculum (30 µl) was removed after 1 h, the monolayer

washed thoroughly and replaced with 200 µl of media containing 2% serum. Media (10 µl) was collected at different time-points (8, 12, 16 and 24 h post-infection) and stored frozen at -70°C , before virus quantification by plaque assay. For cytopathic effect (cpe), PS cell monolayers were infected in 96-well plates at an moi of 1 PFU/cell, in quadruplicates, and stained with naphthalene black after 72 h.

Statistical analysis

Statistical analysis was performed on the data obtained from the virus growth curve studies and the evaluation of cpe in PS cells. For growth curves, the data were plotted to include the standard error of the mean (SEM) for each data set. At any given time point divergence by at least 2 SD from the mean, between wild-type and mutant viruses, was taken as significant. Measurement of cpe was done visually by three independent evaluators in a 'blind' manner. The cpe of viruses were estimated on a scale of 1–4 corresponding to 20–40, 40–60, 60–80 and 80–100% of monolayer destruction following microscopic examination. The interevaluator consistency error was verified using *F*-test which revealed no one evaluation was significantly different from that of the others.

RESULTS

In silico analysis of RNA structures in flaviviruses

Previous *in silico* studies have predicted a stable RNA structure designated SL6, in the C protein-encoding region, for a limited number of viruses within the mTBFV subgroup (16, 26–28). Structural RNA elements were also revealed in the C region of some MBFV (28) although their homology to SL6 of TBFV had not been established. Here, we utilized a variety of independent structure prediction methods and a much larger sample of viral sequences to analyze whether or not the SL6-like structure was conserved throughout the entire genus *Flavivirus*.

In silico analysis of SL6 in the TBFV subgroup

It was found that the overall folding of the first 333 nt of TBFV was highly conserved among several members of the mTBFV subgroup (16, 26–28), with six stable SLs (enumerated 1–6 in Figure 1A). This analysis was extended to investigate the conservation of SL6 in the larger group of distantly related mTBFV, sTBFV and KADV (37). A nucleotide alignment of the C region was generated and optimized by the introduction of numerous gaps (Supplementary Figure S1A); it shows that divergent RFV, GGYV and KSIV (distant virus species of the mTBFV) maintained homology in the SL6 region. However, some nucleotide perturbations in the SL6 region were observed between mTBFV, sTBFV (MEAV, TYUV and SREV) and KADV proving that the region between the initiation codon and SL6 had evolved with frame shifts as we previously demonstrated (16). We conducted MFold analysis to investigate the presence of SL6-like structures in the distantly related mTBFV

(RFV, GGYV and KSIV), sTBFV and KADV groups (Figure 1B).

Despite sequence divergence, all viruses in the mTBFV group formed similar SL6-like structures when the 333 nt or a longer nucleotide region (up to 1000 nt) was used for MFold analysis (data not shown). The SL6-like folds contained a remarkably high number of co-variant and semi-covariant substitutions which maintained the general conformation across divergent viruses (Figure 1B). The minimum free energy dG of folding for SL6 varied between -32.3 and -17.2 kcal/mol with RFV and LIV/GGYV as extremes in this range. Although KADV had a shorter SL6 compared with other TBFVs, the energy of folding was -17.32 kcal/mol, within the range found for mTBFV.

In comparison to SL6 of the mTBFV, the SL6 of sTBFV was shorter and less stable, with a dG in the range -12.5 to -10.6 kcal/mol (Figure 1B). However, the SL6-like structures of sTBFVs were observed as elements of longer and branched RNA conformations (data not shown).

A smaller terminal loop was revealed in the KFDV/AHFV and KSIV sequences resulting in the formation of the tetraloop U(GCCA)A (Figure 1B). The presence of U:A as a loop-closing base pair has been shown to decrease tetraloop stability considerably; in combination with some intraloop sequences this results in intermolecular tensions that prevent the folded tetraloop from achieving a global thermodynamic minimum (38,39). Thus, despite the MFold-mediated predictions, a tetraloop may not form for KFDV/AHFV and KSIV or at least not be sufficiently stable for biologically significant (RNA–RNA or RNA–protein) interactions.

The conservation of a UGCCAA hexanucleotide motif in the terminal loop of SL6 in all the divergent TBFVs was striking. Both TYUV and KADV showed one substitution in the hexanucleotide UGCCUA; TYUV has also lost the first nucleotide (Supplementary Figure S1A).

In the minus-sense orientation, the conservation of an SL6-like structure was not as robust as in the positive-sense. Although most of the TBFVs formed a structure in the minus-sense RNA, the number of hydrogen bonds, the lengths of the stems and free minimal energy of folding varied significantly even between closely related viruses (data not shown). Consequently, the formation of SL6 is likely to be biologically significant only in the positive-sense RNA.

Structure predictions correlated with evidence for SSSV in TBFV genomes (Figure 2). A remarkable drop in SSSV was observed in the SL6 region between positions 209 and 254 of the Vs sequence. The most extreme drop in variability was observed in a window centred on position 221 within the apical stem of SL6. The levels of SSSV within the remainder of the structural protein-encoding region (positions 295–2435) were higher than the upstream portion. Similarly, high levels of SSSV were observed across the non-structural portion of the genome between positions 322 and 2425 (data not shown).

We excluded the possibility that SSSV in the C-coding region was due to codon bias by analyzing nucleotide composition at each position within the codons.

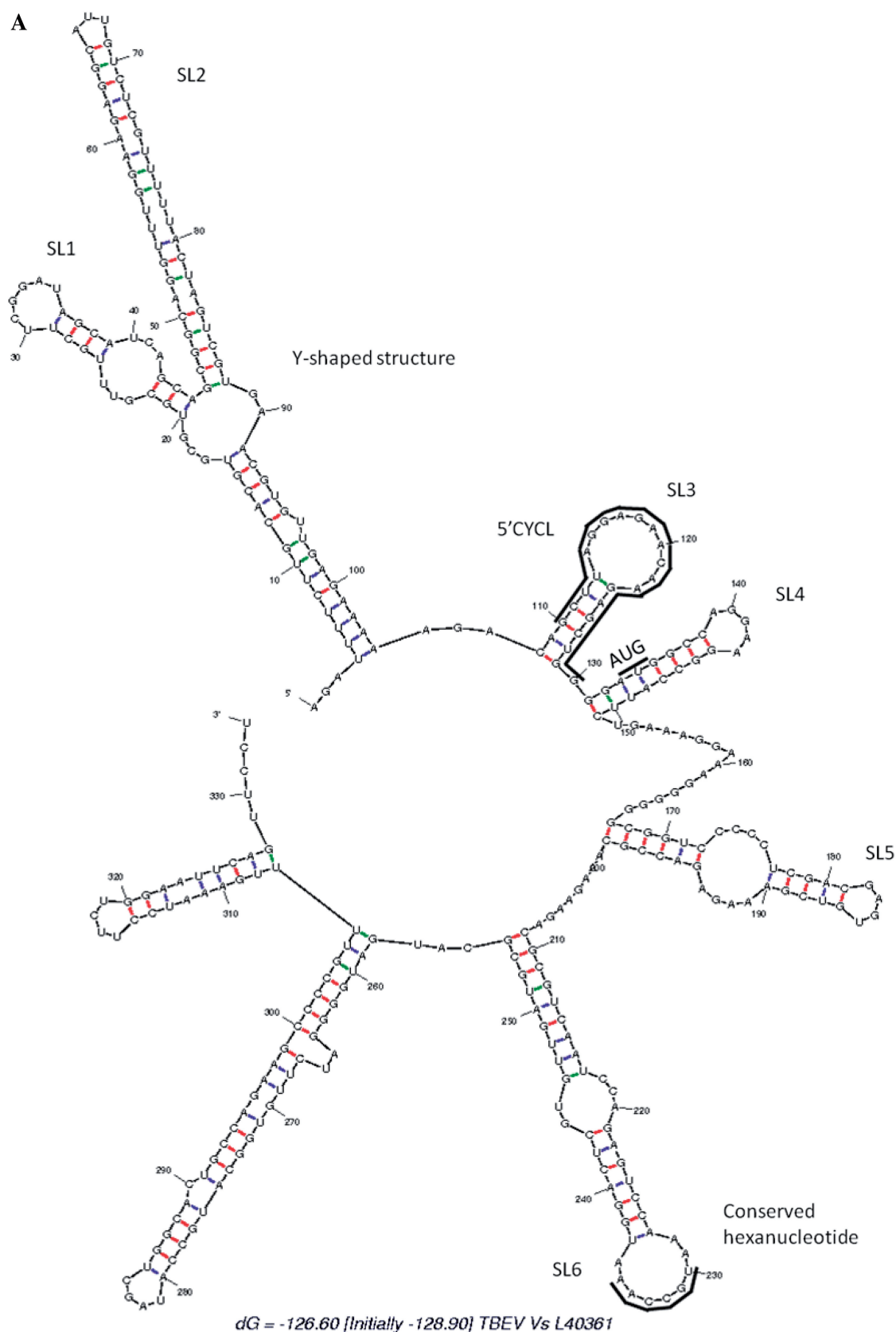


Figure 1. Conservation of SL6 among the TBFVs. (A) Mfold-simulated RNA secondary structure (stable stem loops numerated 1–6) between nucleotides 1–333 of the Vs virus genome. The 5'-CYCL, initiation AUG codon and conserved hexanucleotide UGCCAA are outlined. (B) Comparison of SL6 between TBFV species. Numeration in brackets corresponds to SL6 numbered from the start codon of each virus (abbreviated in Table S1). Free energy dG values of folding are shown in kcal/mol. Covariant and semi-covariant substitutions are underlined on Vs virus.

Continued

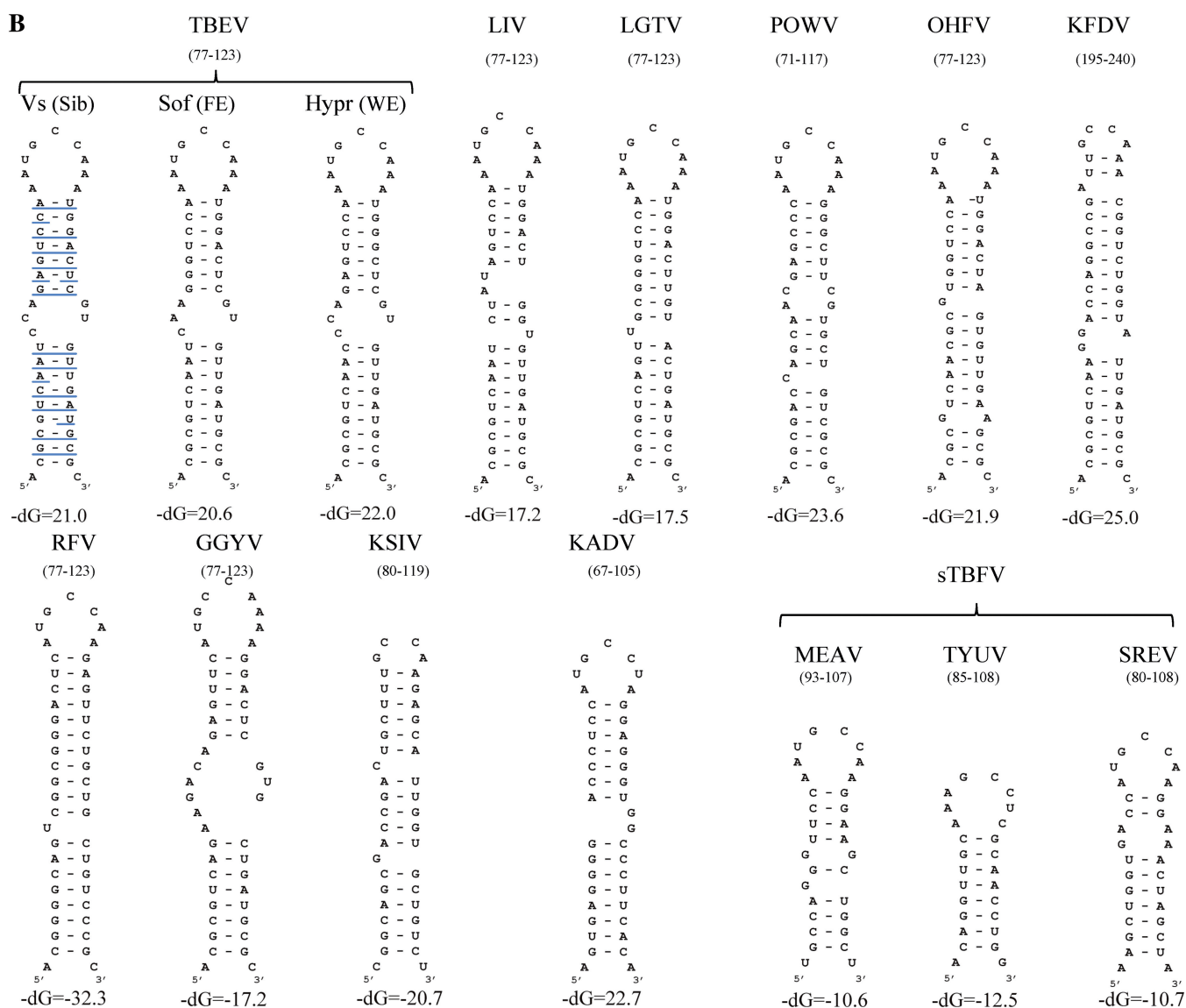


Figure 1. Continued.

No unusual variation of G/C or purine/pyrimidine composition was observed at the third codon position or at positions one or two of the codon (not shown). Likewise, we analyzed the dinucleotide composition at all three possible positions. Although there was a general under-representation of CpG and UpA, and over-representation of CpA and UpG, there was no correlation between areas of SSSV and regions of unusual dinucleotide frequencies (data not shown). These results indicated that evolutionary constraints restrict nucleotide variation within the 5'-coding regions of flavivirus genomes.

The phylogenetic conservation of thermodynamically stable RNA structures across all TBFV group ORFs was further analyzed using the program STRUCTURE_DIST (Figure 2) (40). This method quantifies phylogenetically concordant structures predicted using the widely accepted MFold or UNAFold algorithms, which can then be aligned and overlaid with SSSV results (31,32). Analysis of the entire ORF showed

the most striking evidence for conserved base-pairing between the initiation codon at position 133 and position 318, after which a large drop in the frequency of base-paired nucleotides was observed. Within this region SL6 was predicted to be the most significant structure, with conserved pairing between 209 and 254 centred on a region with a conserved lack of base pairing between positions 228 to 236, representing the unpaired apical loop of SL6. The base-paired stem of SL6 contained conserved short single-stranded regions between positions 218–220 and nucleotides 244 and 245 consistent with the unpaired bulge, either side of the paired stem. This corresponds exactly to the position and structure of SL6 predicted by MFold (Figure 1 and [Supplementary Figure S1A](#)).

In silico prediction of SL6 in the MBFV group

An annotated nucleotide alignment of the C-coding region between TBFV and three MBFV groups (JEV, DENV

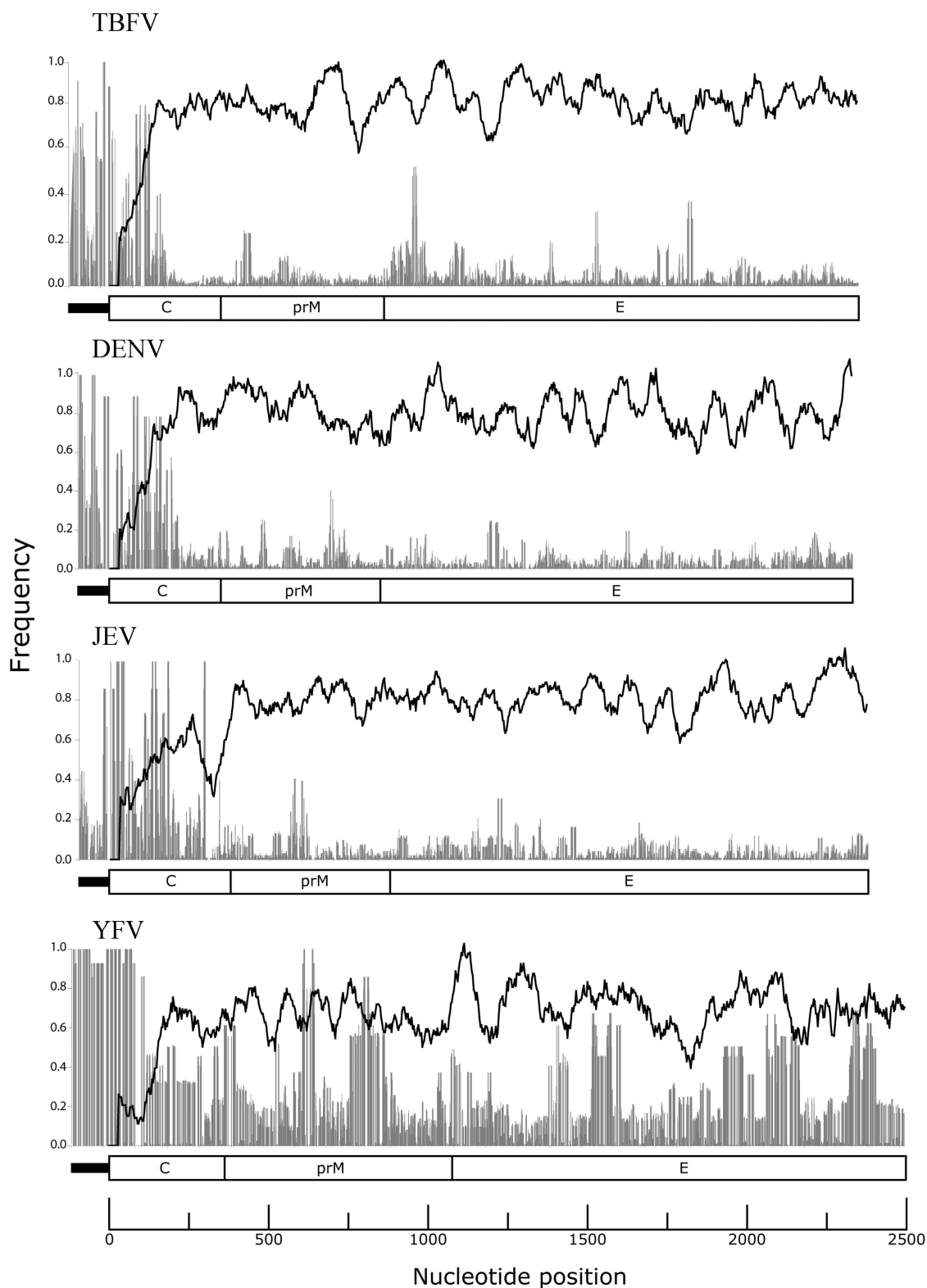


Figure 2. Phylogenetic conservation of RNA structures in the TBFV and MBFV groups across the 5'-UTR and structural protein coding regions. Black lines represent SSSV for TBFV, DENV, JEV and YFV. Gray filled bars represent phylogenetic conservation of base pairing from a STRUCTURE_DIST pair-wise comparison of connect files generated by MFold.

and YFV) was constructed based on a previously presented alignment (16) but modified to include newly sequenced distantly related mTBFV, sTBFV and KADV isolates (Supplementary Figure S1A). The C protein TBFV/MBFV alignment (available on request) was used to anchor the divergent nucleotide sequences. The annotations include the 5'-CYCL of MBFV, an 8-nt long cyclisation domain highly conserved between all MBFVs (16). The 5'-CYCL interacts with a complementary sequence 3'-CYCL in the 3'-UTR to form a dsRNA panhandle, a vital element of the replication promoter that initiates viral RNA synthesis (16). For the TBFV the 21-nt long 5'-CYCL is located in the 5'UTR (i.e. outside the alignment in Supplementary Figure S1A; highlighted in Figure 1A). The 5'-CYCL for MBFV mapped to the capsid gene and, among the TBFV, aligns optimally with a region that is identified only in TUYV (Supplementary Figure S1A).

Nucleotide sequence homology was observed between the TBFVs and MBFVs particularly in the SL6 region of some JEV group viruses. For example, WNV was observed to share both the stem and loop sequences of TBFV SL6 (Supplementary Figure S1A). It is of note that the SL6-like region of MBFV maps directly downstream of the highly conserved 5'CYCL (Supplementary Figure S1A).

MFold was used to test the ability of these regions to form SL6-like structures within each MBFV group and the stem and loop elements of these SL6-like structures were superimposed onto the TBFV/MBFV alignment (Supplementary Figure S1A). This comparison revealed that structures predicted within each MBFV group show not only sequence but also structural homology with SL6 of the TBFV group. This alignment was further annotated with RNA structures predicted by the ALIDOT-based analysis of entire flavivirus genomes of 11 000 nt (28), i.e. JE2, JE3 and JE4 for JEV; DV2 and DV3 for DENV and YF4 for YFV (Supplementary Figure S1A). For all MBFVs with the exception of YFV the MFold predictions were somewhat different from those made using ALIDOT, most likely due to the shorter length of the regions (60–80 nt) used for the MFold analysis. Additional statistical methods, SSSV and STRUCTURE_DIST were used to assess the conservation of the SL6 homologous structures for each of the major MBFV groups (Figure 2).

For the JEV group the mean SSSV between positions 117–358 (start codon at position 97) was consistent with ALIDOT-predicted RNA structures JE2, JE3 and JE4 (Supplementary Figure S1A) (28). However, the SL6-like structure for the JEV group was clearly predicted by STRUCTURE_DIST analysis (brown box in Supplementary Figure S1A), in accordance with MFold and alignment analysis.

For the DENV subgroup, a marked region of SSSV was revealed in the C-coding region between positions 155–257 (start codon at position 95) when compared with the rest of the structural coding region (Figure 2), consistent with RNA structure DV3 previously predicted between nucleotides 163–183 (28) (Supplementary Figure S1A). Both ALIDOT-predicted DV2 and DV4 (28) fall

immediately either side of the region of maximum SSSV suggesting that they are less conserved than DV3 (Supplementary Figure S1A). STRUCTURE_DIST also predicts the formation of the DV2 and DV3 but not the SL6-like structure (Supplementary Figure S1A and Figure 2). However, a truncated SL6-like structure was predicted to form in all DENV serotypes, albeit at a sub-optimal energy level, when the SL6-like region was folded independently from neighboring regions that form more stable overlapping structures (Supplementary Figure S1A). Taken together, these data indicate that the DENV SL6-like structure was the least stable conformation among the MBFVs, potentially preventing its prediction by statistical approaches used here and elsewhere (28). Despite this, the short-stem region of putative DENV SL6-like structures is highly conserved within the DENV group (DENV serotypes 1–4) and also between DENV and JEV (Supplementary Figure S1A) suggesting that a linear or conformational signal at this location might have some functionality.

A similar restriction in SSSV was observed in the YFV C-coding region, with maximum SSSV corresponding to the ALIDOT-predicted structure YF4 (Figure 2) (28). Among the MBFVs, only the YFV SL6-like structure was predicted by both thermodynamic and phylogenetic methods.

In summary, a proximally truncated SL6-like structure was predicted in all MBFV groups, although it was less stable in the DENV group, particularly the DENV3 serotype.

***In silico* prediction of SL6 in the NKV and PABV groups**

In contrast to TBFV and MBFV, the NKV and PABV groups are not arboviruses and their replication is limited to only one natural host, i.e. rodents/bats (NKV) or mosquitoes (PABV). The high nucleotide divergence (Supplementary Figure S1B and S1C) and limited number of complete published sequences for members of the NKV and PABV groups precluded the use of both phylogenetic and thermodynamic approaches to RNA structure prediction. When MFold analysis was performed with available sequences, no thermodynamically stable RNA structures were observed in the region corresponding to the TBFV SL6 region. However, an SL6-like structure, with a similar apical loop CCAA motif was observed in KRV (PABV), upstream of the analogous TBFV SL6.

Experimental evidence supporting the predicted structure ISL6

Strategy of mutagenesis on stem-loop 6. Initial design of mutations focused on synonymous codon positions. However, in all but a few instances, this was limited due to the distinctive sequence organization of the apical loop and base paired stem. The first and third codons of the conserved MPN tripeptide (loop region) are limited in respect of variation; M could not be changed and N has two possible silent variations both of which are outside the apical loop (Figure 3). Consequently, when mutating the terminal loop sequence UGCCAAU, silent substitutions

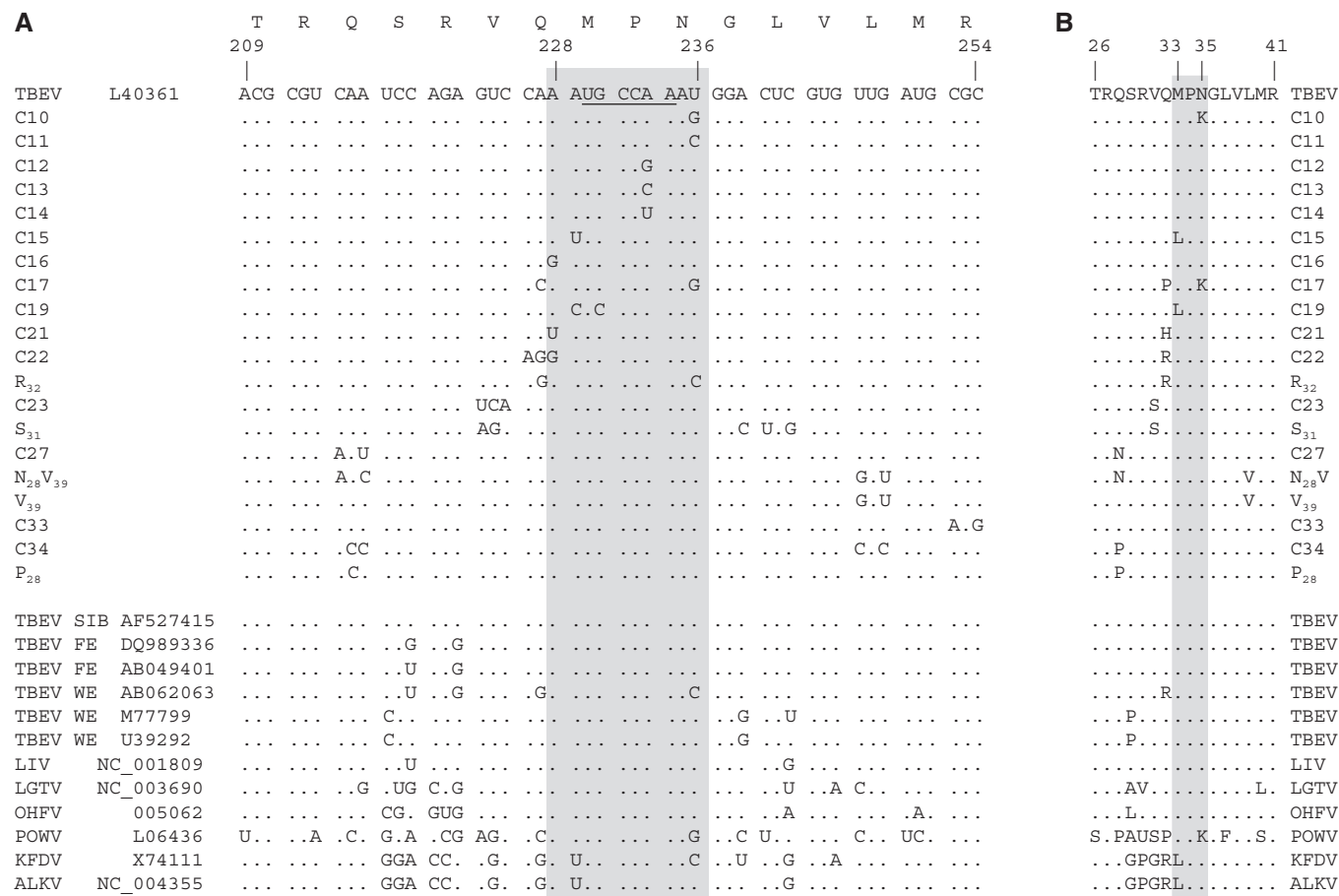


Figure 3. Site-directed mutagenesis of SL6. Nucleotide (A) and amino acid (B) alignments of SL6 sequences within C gene of mTBFV and mutants produced from the infectious clone of TBEV. Viruses are specified in [Supplementary Table S1](#). Sequence of Vs virus is on the top; nucleotide and amino acid substitutions are shown by letters. The conserved hexanucleotide UGCCAA is underlined. SL6 region is located between nucleotides 209 and 254 and amino acids 26–41 of the Vs virus genome. Unpaired terminal loop of SL6 is highlighted by a gray box.

could only be introduced into the P codon. Similar difficulties were encountered with mutagenesis of the stem, in which the vast majority of possible synonymous and non-synonymous mutations resulted in no significant conformational changes. The MFold-simulated folding of numerous SL6-mutants revealed a high level of evolutionary ‘protection’ of SL6 against spontaneous single mutations (not shown) and provides additional evidence for the maintenance of SL6 functionality.

In order to resolve the difficulties with design of mutations, three different approaches were adopted (Figure 3). First, we introduced all possible silent substitutions, to target the conserved hexanucleotide and the stem (mutants C12, C13, C14, C16 and C33). Second, we introduced mutations (C10, C15, C17, C19 and C34) that mimicked ‘natural’ amino acid substitutions observed in this region of other mTBFV spp. Third, as a control for mutations that changed amino acids we also introduced compensatory substitutions encoding the same mutated amino acids while restoring the SL6 structure. Accordingly, mutations R32, S31, N₂₈, V₃₉, V₃₉ and P₂₈ were designed as controls for non-synonymous mutants C22, C23, C27 and C34 (Figure 3).

The predicted impact of each substitution (Figure 3) on the secondary structure of SL6 is shown in Figure 4. The plaque characteristics, cpe and growth dynamics of each mutant compared with those of original pGGVs virus (Table 1 and Figure 5). Single-step growth curves revealed differences of ~1 log₁₀ between the mutants early after infection (12–16 h p.i.) which were reproducible and statistically significant (Figure 5).

To exclude the effect of spontaneous mutations in the 5′- and 3′-UTRs which contain TBFV promoter and enhancer elements (16) that might compensate for the effect of the SL6-mutations, rescued virus was not passaged prior to phenotype evaluation and key regions of the genome (1–940 and 10206–10927) were sequenced following recovery of each SL6-mutated virus. Only the intended substitutions were present, with no reversions or other compensatory mutations were observed. The effect of each mutation (reduction from large wild-type plaques of the pGGVs virus to medium, small or pin pointed) was scored if the SL6-mutated strain contained >90% of plaques with the altered morphology. The presence of a minor plaque population (between 1 and 10%) was considered as the inevitable result of the variation inherent

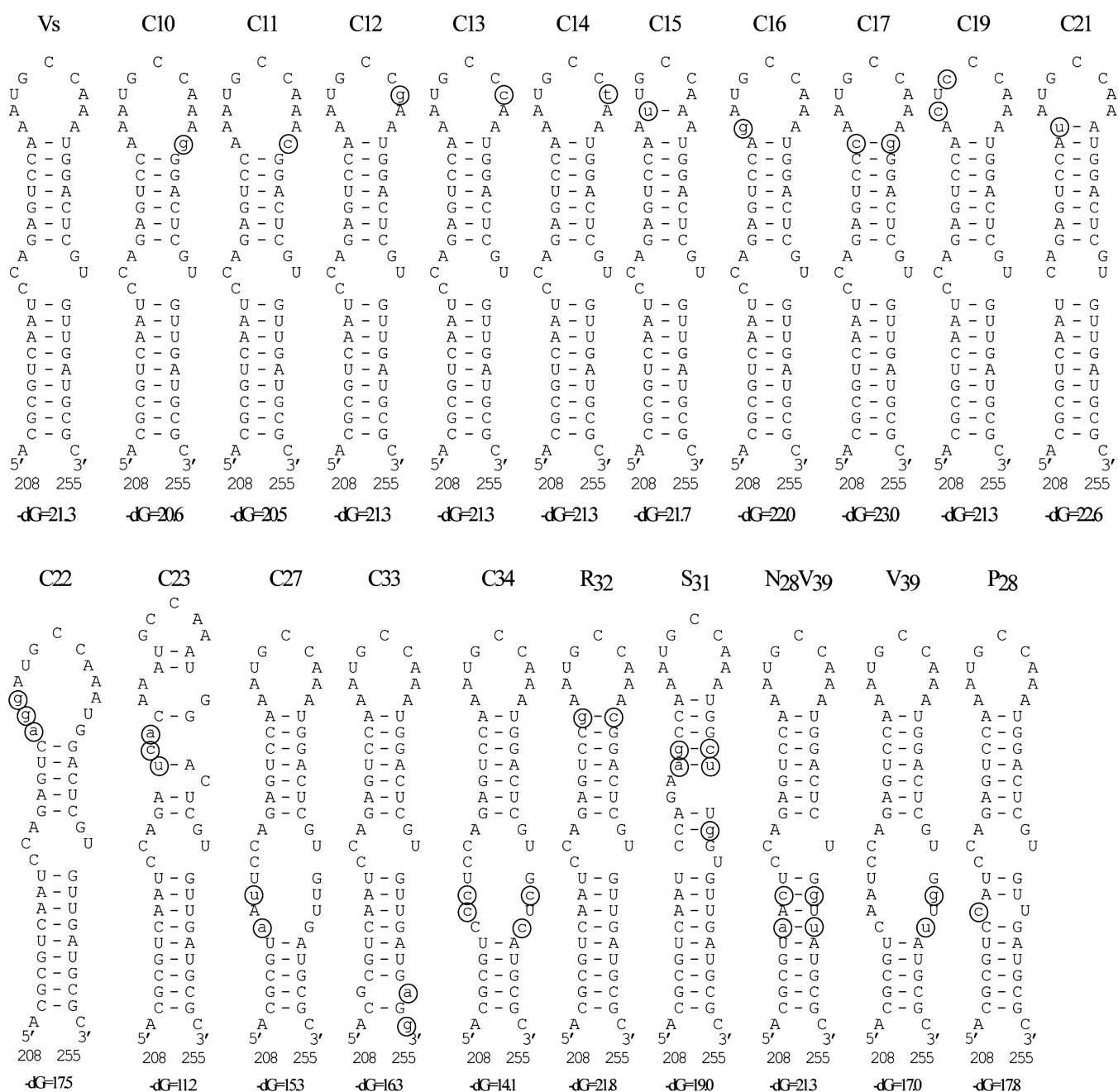


Figure 4. Effect of point mutations on SL6 conformation as predicted by Mfold. Point mutations are shown in circles. Names of the mutants are indicated on the top. Free ΔG energy of folding is indicated underneath each structure.

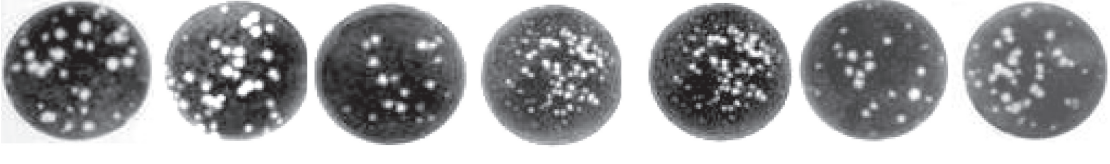

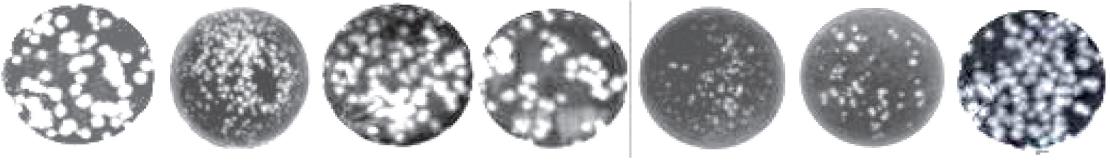
in all RNA viruses, the consequence of a high error rate in the virus RdRp (41).

Sequence changes in the apical loop of SL6. In mutants C12, C13, C14, C16 and C19 substitutions within the apical loop changed the nucleotide sequence without altering the overall conformation (Figures 3 and 4). Four of these mutations C12, C13, C14 and C19 were introduced into the conserved hexanucleotide UGCCAA. Silent mutations C12, C13 and C14 changed plaque morphology; the C13 and C14 mutants that contain purine-to-pyrimidine substitutions also showed reduced

growth characteristics and cpe (Table 1 and Figure 5). Silent substitution C16, located outside the conserved hexanucleotide in SL6, did not affect the virus phenotype.

Two purines were changed for two pyrimidines in mutant C19, one in the conserved hexanucleotide. This mutant was highly attenuated in cell culture producing no cpe and a small turbid plaque phenotype (Figures 3–5 and Table 1). These two purine–pyrimidine substitutions resulted in the amino acid substitution $M_{33} \rightarrow L$ that mimicked the corresponding natural amino acid in KFDV and AHFV (Figure 3). Nevertheless, $M_{33} \rightarrow L$, mutant C15, produced by different nucleotide

Table 1. Affect of mutations within the SL6 on TBEV phenotype

Virus	pGGVs	C10	C11	C12	C13	C14	C15
Nt/AA*	Wild type	T ₂₃₇ G/ N ₃₅ K	T ₂₃₇ C	A ₂₃₄ G	A ₂₃₄ C	A ₂₃₄ T	A ₂₂₉ T/ M ₃₃ L
Plaque phenotype	Large/bright	Large/bright	Large/bright	Small/bright	Small/bright	Medium/turbid	Medium/turbid
Plaque morphology							
CPE	4	4	4	4	3	2	2
Virus	C16	C17	C19	C21	C22	R ₃₂	C23
Nt/AA*	A ₂₂₈ G	A ₂₂₇ C/ Q ₃₂ P T ₂₃₇ G/ N ₃₅ K	A ₂₂₉ C/ M ₃₃ L G ₂₃₁ C	A ₂₂₈ T/ Q ₃₂ H	C ₂₂₆ A/ Q ₃₂ R A ₂₂₇ G A ₂₂₈ G	A ₂₂₇ G/ Q ₃₂ R T ₂₃₇ C	G ₂₂₃ T/ V ₃₁ S T ₂₂₄ C C ₂₂₅ A
Plaque phenotype	Large/bright	Large/bright	Pinpoint/turbid	Medium/turbid	Medium, turbid	Large, bright	Pinpoint, turbid
Plaque morphology							
CPE	4	3	1	3	3	4	2
Virus	S ₃₁	C27	N ₂₈ V ₃₉	V ₃₉	C33	C34	P ₂₈
Nt/AA*	G ₂₂₃ A / V ₃₁ S T ₂₂₄ G; A ₂₄₀ C; C ₂₄₁ T; C ₂₄₃ G	C ₂₁₄ A/ Q ₂₈ N A ₂₁₆ T	C ₂₁₄ A/ Q ₂₈ N T ₂₄₇ G/ L ₃₉ V G ₂₄₉ T; A ₂₁₆ C	T ₂₄₇ G / L ₃₉ V G ₂₄₉ T	C ₂₅₃ A C ₂₅₅ G	A ₂₁₅ C / Q ₂₈ P A ₂₁₆ C; T ₂₄₇ C; G ₂₄₉ C	A ₂₁₅ C/ Q ₂₈ P
Plaque phenotype	Large, bright	Pinpoint, turbid	Large, bright	Large, bright	Pinpoint turbid	Pinpoint turbid	Large, bright
Plaque morphology							
CPE	4	2	4	4	1	1	4

Plaque size for each mutant was defined as large (5–6 mm), medium (3–4 mm), small (1–2 mm) or pinpoint (>1 mm). Some plaques, in comparison with parent Vs virus, were described as turbid. The cpe produced by each mutant in comparison to the wild-type virus was evaluated on a scale of 0–4 where 0 indicates no cpe and 4 is maximum cpe (i.e. 80% cell lysis as observed for the control pGGVs virus) in five repeated experiments, each in quadruplicates. Nt/AA* - Nucleotide/amino acid substitutions.

substitutions had only a moderate effect on virus replication (below). Therefore, the biological consequences of mutation C19 may be attributed, at least partially, to the nucleotide substitutions.

Conformational changes to the apical loop of SL6. Mutations C10, C11, C15, C21, C22 and C23 changed the shape of the loop and base-paired stem within SL6 (Figure 4). Replication of mutant C10 (with an enlarged loop and shortened stem) and C17 (restored

wild type conformation due to the second compensatory mutation) was delayed in the early stage of the infection cycle; C17 caused slightly reduced cpe but the plaque morphology of both was equivalent to that of the parental pGGVs virus (Figure 5 and Table 1). The minor phenotypic changes resulting from these mutations could be explained by the accompanying amino acid substitutions N₃₅→K and Q₃₂→P imitating POWV (Figure 3). However, a silent substitution A₂₃₄→G that also enlarged the apical loop of mutant C11 (Figure 4)

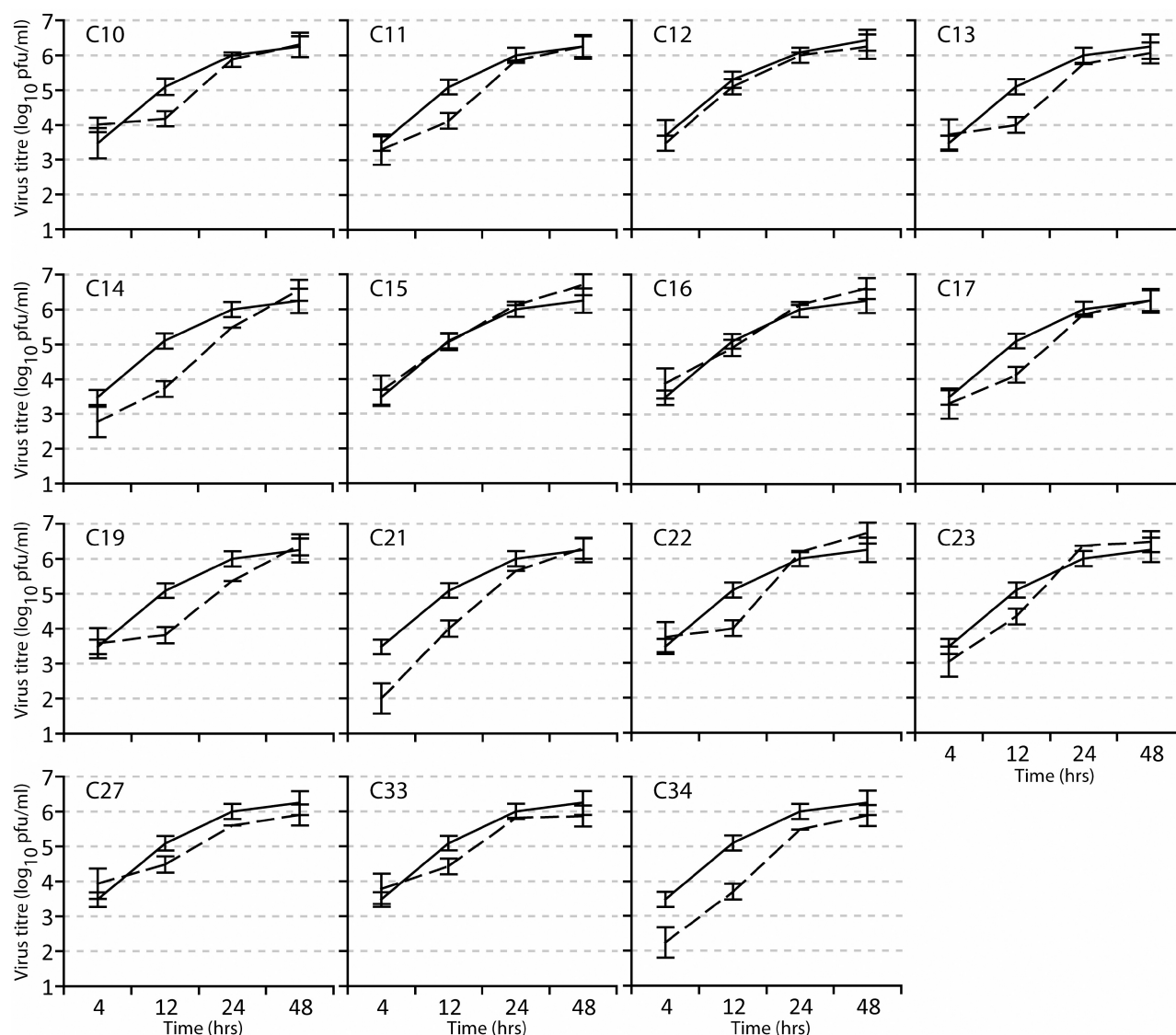


Figure 5. Affect of mutations within SL6 on TBEV replication kinetics, measured by growth curves over time. The PS cells were infected with control pGGVs (solid line) and SL6-mutant virus (dashed lines) at an moi 1 PFU/cell and supernatant medium was collected at time-points 8, 12, 16 and 24 h post-infection (axis *x*). The virus titres (\log_{10} PFU/ml; axis *y*) were estimated by plaque assay. Each curve represents the average value of virus titre estimated in four parallel experiments, repeated twice. Error bars represent 2 SD from the mean.

caused similar biological effects; it did not affect virus plaque size or level of cpe, but reduced virus replication rate early after infection (Figure 5 and Table 1).

Mutation C15, which shortened the apical loop (Figure 4), did not affect virus growth but changed the plaque morphology and delayed the development of cpe (Table 1 and Figure 5). The C15 mutation altered the amino acid $M_{33} \rightarrow L$, which imitates the KFDV/AHFV group (Figure 3), potentially contributing to the observed biological effect. Mutation C21 that reduced the apical loop size (Figure 4) interfering with exposure of the hexanucleotide, also had a moderate affect on virus growth although the accompanying effect of amino acid substitution $Q_{32} \rightarrow H$ (Figure 3) cannot be excluded (Table 1 and Figure 5).

Mutant C22 contained three substitutions that considerably increased the size of the apical loop thus shortening

the base paired stem. Three nucleotide substitutions present in mutant C23 had the opposite affect in shrinking the apical loop (Figures 4). Both C22 and C23 had altered growth dynamics, plaque morphology and cpe (Table 1 and Figure 5). The nucleotide substitutions of both led to amino acid substitutions $Q_{32} \rightarrow R$ and $V_{31} \rightarrow S$, respectively. To exclude their influence on virus growth, counterpart 'control' mutants R_{32} and S_{31} were analyzed, with the same amino acid substitutions but without alteration of the SL6 conformation (Figures 3 and 4). Both of these control mutants exhibited wild-type plaque morphology and cpe characteristics (Table 1).

Substitutions in the stem of SL6. Three mutants were designed to investigate the influence of SL6 stem length. Most attempts to design synonymous substitutions had little effect on the stem folding conformation. Only silent

mutant C33 (C₂₅₃→A and C₂₅₅→G) exhibited a significantly shortened duplex stem, with a corresponding elevated level of dG folding energy. These positions are highly conserved among the mTBFV (Figure 3) and, as expected, had a profound effect on virus replication; C33 displayed pinpoint plaques, reduced growth characteristics and almost no cpe (Table 1 and Figure 5).

Two other mutants C27 and C34 had shortened stems due to the formation of a large internal bulge (Figure 4), and exhibited profoundly altered biological characteristics (Table 1 and Figure 5). However, C27 and C34 included amino acid substitutions Q₂₈→N and Q₂₈→P, respectively, the latter resembling POWV (Figure 3). To rule out the amino acid change as influential, two mutants were designed as a control for C27; double mutant N₂₈V₃₉ and single mutant V₃₉, neither of which affected SL6 conformation (Figure 4). Similarly mutant P₂₈, a control for C34, contained the same amino acid substitution Q₂₈→P but maintained SL6 conformation (Figures 3 and 4). All three control mutants, N₂₈V₃₉, V₃₉ and P₂₈, displayed wild-type large plaque phenotype and cpe (Table 1).

DISCUSSION

In a previous study using MFold-simulated RNA structures for a limited number of mTBFV species, we predicted the existence of SL6 in the C-coding region of TBFV. A conserved hexanucleotide UGCCAA in the apical loop and compensatory mutations in the duplex stem of the SL6 implied the formation of the stable RNA structure in ORF of the TBFV genomes (26,27). However, contradicting these findings a deletion within the C-coding region, which included SL6, did not prevent recovery of viable, albeit attenuated, TBEV (42). In this study, we employed a variety of complementary phylogenetic and thermodynamic methods to examine the evolutionary conservation of SL6 using a much larger sample of significantly divergent TBFVs, including new members of the mTBFV, sTBFV and Kadam subgroups (37). The viruses in the other ecological groups, namely MBFV, NKV and PABV were also included in this analysis to trace the evolution of SL6 throughout the entire genus *Flavivirus*. In addition, we used a reverse genetic system (34,36) to engineer TBEV strains with mutated SL6 to reveal the biological significance of this structure.

Thermodynamic and phylogenetic analysis of large sequence data sets indicated that all TBFVs including even the distantly related mTBFV, KADV and sTBFV form an SL6-like structure with an exposed conserved hexanucleotide although the molecular details of the predicted stem-loop varied among the mTBFV, sTBFV and KADV subgroups (Figure 1B). In similar manner, an SL6-like structure has been predicted for MBFV although with less stability in comparison to SL6 in TBFV. Two other flavivirus groups NKV and PABV demonstrated no significant sequence homology with the TBFV SL6 region although the genome of KRV (PABV group) formed a thermodynamically stable structure in

close vicinity to the TBFV SL6 with a similar terminal loop motif CCAA (TBFV—UGCCAA) (Supplementary Figure S1).

To test the biological significance of SL6 in the TBFV group we engineered 21 mutant viruses with point mutations that altered the linear sequence of the unpaired apical loop or destabilized the base-paired stem. Substitutions within the conserved hexanucleotide loop down-regulated virus growth kinetics whereas changes in the terminal loop outside the hexanucleotide sequence did not alter the observed phenotype. The most significant changes of virus phenotype resulted from substitutions that distorted the stem of SL6; mutations that influenced the length or stability of the stem resulted in the recovery of viruses that formed small and/or turbid plaques. Increasing or decreasing the size of the apical loop had a minor biological effect on virus replication although this could also be interpreted as an effect of the altered stem length. However, the changes in replication kinetics from all modifications of SL6 were moderate and manifested themselves predominantly during the early stage of the virus replication cycle (Table 1).

Previous analysis of RNA secondary structure across the *Flavivirus* genus led to the concept of promoter and enhancer elements that initiate assembly of the virus polymerase complex (16–18,23,27,43,44). Enhancers were identified as RNA structures that individually produce only small biological effects on virus replication. However, the significance of enhancers as targets for the attenuation of flaviviruses to engineer live vaccines is evident from the example of dengue virus (24,25). Moreover, sequence and structural conservation of flavivirus enhancers is consistent with a role as key players in virus survival in the natural environment. We previously proposed that the cumulative action of several enhancer elements could contribute significantly to the overall rate of assembly of polymerase complexes, thereby enhancing virus survival across a range of natural hosts (17,18,23,27,43,44). In this respect, the presented experimental data indicate that SL6 belongs to the category of REEs, i.e. RNA structures that accelerate the replication of viruses (45–56). This eliminates the apparent contradictions between extremely high levels of SL6 conservation across divergent TBFV virus species and the redundancy of this element for the replication of laboratory-maintained TBEV strains (45–56). However, the specific mechanism by which SL6 functions to enhance virus replication remains to be elucidated.

It has recently been demonstrated that a short but highly conserved RNA hairpin (sHP) localized in the 3'-UTR of DENV2 RNA regulates the transition from a circular (required for the initiation of RNA replication) to linear RNA form during the progress of viral RNA synthesis (57). The SL6-like structure of MBFV is localized immediately downstream of the 5'-CYCL (i.e. within the capsid gene, Supplementary Figure S1A) suggesting it could also contribute to genome circularization. It is possible that in accord with the 3' sHP (highly conserved throughout the genus *Flavivirus*), it contributes to the unpairing of the 5'-3'-CYCL panhandle, to promote RNA elongation on the linear template. In contrast, the

5'-CYCL of TBFV is mapped to the 5'-UTR (i.e. upstream of the capsid gene, Figure 1A) and therefore other tentative functions of the TBFV SL6 are not excluded, such as enhancing virus translation, RNA replication or playing a role in regulation between these processes; the possibility of a kissing-loop enhancer of genome circularization was previously discussed (17,18,23,27,43,44).

The C protein of flaviviruses is highly basic at the N-terminus, specifically binding virus genomic RNA during encapsidation and plausibly acting as an RNA chaperone as shown for other viruses (58). The sequence of SL6 within the C coding region localizes to the junction of the positively charged domain and a following hydrophobic domain that interacts with the virus envelope proteins during assembly (42). It is possible that additional synonymous codon flexibility may be accommodated in this region due to the requirement to conserve the charge or hydrophobic characteristics of the domain, rather than any specific amino acid sequence.

Although our studies provide support for the REE role of SL6 in TBEV it is unclear if SL6-like structures of MBFV act similarly as functionally significant REE. However, the remarkable resemblance of the WNV SL6-like structure to TBFV SL6 suggests that it might serve a similar function, at least in one virus group. However, a final conclusion for the MBFV and also for the more distant NKV or PABV groups is not possible ahead of further functional studies.

Being arboviruses, MBFVs and TBFVs are adapted for transmission between distantly related vertebrate hosts and invertebrate vectors. The requirement to adapt to different molecular environments might result in the evolution of enhancer elements essential for virus replication in one host while being redundant in another. This could explain the contradiction between strict conservation of the different flavivirus enhancers and their apparent redundancy in laboratory systems, which are largely based on mammalian cells (17,18,23,27,43,44). Mutations in SL6 described here have demonstrated its enhancer properties in mammalian cells and it will be interesting to evaluate SL6 enhancer activity in ticks, the major host for maintenance of the TBFV group in the environment (59–61).

In conclusion, bioinformatic analysis demonstrated the presence of a conserved RNA secondary structure in the C coding region of the divergent TBFV group. Disruption of this structure compromised virus replication implying an REE function for SL6. By homology with the TBFVs, SL6-like structures were observed in the genomes of some MBFVs and plausibly indicate a similar role as replication enhancers. Future studies using sub-genomic replicons will allow direct measurement of the influence of these sequences on RNA replication and on interaction with viral and host proteins.

SUPPLEMENTARY DATA

Supplementary Data are available at NAR Online.

ACKNOWLEDGEMENTS

We thank M. Armesto for technical assistance in the experimental part of the project and Prof. Peter Simmonds for technical assistance in the bioinformatics and critical reading of the manuscript.

FUNDING

The Biotechnology and Biological Sciences Research Council grant BBS/B/00697, the Sixth European Union Framework grant (VIZIER EU Contract LSHG-CT-2004-511960); Medical Research Council grant (ID 87652 to T.S.G. and I.M.J.); M.R.C. support (to D.J.E.). Funding for open access charge: Medical Research Council grant (ID 87652)

Conflict of interest statement. None declared.

REFERENCES

- Gritsun, T.S., Nuttall, P.A. and Gould, E.A. (2003) Tick-borne flaviviruses. *Adv. Virus Res.*, **61**, 317–371.
- Gritsun, T.S., Lashkevich, V.A. and Gould, E.A. (2003) Tick-borne encephalitis. *Antiviral Res.*, **57**, 129–146.
- Suss, J. (2008) Tick-borne encephalitis in Europe and beyond—the epidemiological situation as of 2007. *Euro. Surveill.*, **13**, 1–7.
- Heinz, F.X., Collett, M.S., Purcell, R.H., Gould, E.A., Howard, C.R., Houghton, M., Moormann, R.J.M., Rice, C.M. and Thiel, H.J. (2000) Family *Flaviviridae*. In M.H.V., Fauquet, R., Bishop, C.M., Carstens, D.H.L., Estes, E., Lemon, M.K., Maniloff, S., Mayo, J., McGeoch, M.A., Pringle, D.C.R. *et al.* (eds), *Virus Taxonomy. 7th International committee for the Taxonomy of Viruses*. Academic Press, San Diego, pp. 859–878.
- Crabtree, M.B., Sang, R.C., Stollar, V., Dunster, L.M. and Miller, B.R. (2003) Genetic and phenotypic characterization of the newly described insect flavivirus, Kamiti River virus. *Arch. Virol.*, **148**, 1095–1118.
- Cammisa Parks, H., Cisar, L.A., Kane, A. and Stollar, V. (1992) The complete nucleotide sequence of cell fusing agent (CFA): Homology between the nonstructural proteins encoded by CFA and the nonstructural proteins encoded by arthropod-borne flaviviruses. *Virology*, **189**, 511–524.
- Hoshino, K., Isawa, H., Tsuda, Y., Yano, K., Sasaki, T., Yuda, M., Takasaki, T., Kobayashi, M. and Sawabe, K. (2007) Genetic characterization of a new insect flavivirus isolated from *Culex pipiens* mosquito in Japan. *Virology*, **359**, 405–414.
- Gritsun, T.S. and Gould, E.A. (2008) In Mahy, B.W.J. and van Regenmortel, M.H.V. (eds), *Encyclopedia of Virology*, Vol. 5, 3rd edn. Elsevier, Oxford, pp. 45–54.
- Hahn, C.S., Hahn, Y.S., Rice, C.M., Lee, E., Dalgarno, L., Strauss, E.G. and Strauss, J.H. (1987) Conserved elements in the 3' untranslated region of flavivirus RNAs and potential cyclization sequences. *J. Mol. Biol.*, **198**, 33–41.
- Cahour, A., Pletnev, A., Vazille Falcoz, M., Rosen, L. and Lai, C.J. (1995) Growth-restricted dengue virus mutants containing deletions in the 5' noncoding region of the RNA genome. *Virology*, **207**, 68–76.
- Khromykh, A.A., Meka, H., Guyatt, K.J. and Westaway, E.G. (2001) Essential role of cyclization sequences in flavivirus RNA replication. *J. Virol.*, **75**, 6719–6728.
- Corver, J., Lenches, E., Smith, K., Robison, R.A., Sando, T., Strauss, E.G. and Strauss, J.H. (2003) fine mapping of a cis-acting sequence element in yellow fever virus rna that is required for RNA Replication and cyclization. *J. Virol.*, **77**, 2265–2270.
- Filomatori, C.V., Lodeiro, M.F., Alvarez, D.E., Samsa, M.M., Pietrasanta, L. and Gamarnik, A.V. (2006) A 5' RNA element promotes dengue virus RNA synthesis on a circular genome. *Gene. Dev.*, **20**, 2238–2249.

14. Kofler, R.M., Leitner, A., O'Riordan, G., Heinz, F.X. and Mandl, C.W. (2003) Spontaneous mutations restore the viability of tick-borne encephalitis virus mutants with large deletions in protein C. *J. Virol.*, **77**, 443–451.
15. Kofler, R.M., Hoenninger, V.M., Thurner, C. and Mandl, C.W. (2006) Functional analysis of the tick-borne encephalitis virus cyclization elements indicates major differences between mosquito-borne and tick-borne flaviviruses. *J. Virol.*, **80**, 4099–4113.
16. Gritsun, T.S. and Gould, E.A. (2007) Origin and evolution of flavivirus 5'UTRs and panhandles: trans-terminal duplications? *Virology*, **366**, 8–15.
17. Gritsun, T.S. and Gould, E.A. (2006) The 3' untranslated region of tick-borne flaviviruses originated by the duplication of long repeat sequences within the open reading frame. *Virology*, **350**, 269–275.
18. Gritsun, T.S. and Gould, E.A. (2007) Origin and evolution of 3'UTR of flaviviruses: long direct repeats as a basis for the formation of secondary structures and their significance for virus transmission. *Adv. Virus Res.*, **69**, 203–248.
19. Men, R., Bray, M., Clark, D., Chanock, R.M. and Lai, C.J. (1996) Dengue type 4 virus mutants containing deletions in the 3' noncoding region of the RNA genome: analysis of growth restriction in cell culture and altered viremia pattern and immunogenicity in rhesus monkeys. *J. Virol.*, **70**, 3930–3937.
20. Mandl, C.W., Holzmann, H., Meixner, T., Rauscher, S., Stadler, P.F., Allison, S.L. and Heinz, F.X. (1998) Spontaneous and engineered deletions in the 3' noncoding region of tick-borne encephalitis virus: construction of highly attenuated mutants of a flavivirus. *J. Virol.*, **72**, 2132–2140.
21. Bredenbeek, P.J., Kooi, E.A., Lindenbach, B., Huijckman, N., Rice, C.M. and Spaan, W.J. (2003) A stable full-length yellow fever virus cDNA clone and the role of conserved RNA elements in flavivirus replication. *J. Gen. Virol.*, **84**, 1261–1268.
22. Tilgner, M., Shi, P.Y., Lo, M.K. and Bernard, K.A. (2004) Structure and function of the 3' terminal six nucleotides of the west Nile virus genome in viral replication. *J. Virol.*, **78**, 8159–8171.
23. Gritsun, T.S. and Gould, E.A. (2006) Direct repeats in the 3' untranslated regions of mosquito-borne flaviviruses: possible implications for virus transmission. *J. Gen. Virol.*, **87**, 3297–3305.
24. Romero, T.A., Tumban, E., Jun, J., Lott, W.B. and Hanley, K.A. (2006) Secondary structure of dengue virus type 4 3' untranslated region: impact of deletion and substitution mutations. *J. Gen. Virol.*, **87**, 3291–3296.
25. Blaney, J.E. Jr, Sathe, N.S., Goddard, L., Hanson, C.T., Romero, T.A., Hanley, K.A., Murphy, B.R. and Whitehead, S.S. (2008) Dengue virus type 3 vaccine candidates generated by introduction of deletions in the 3' untranslated region (3'-UTR) or by exchange of the DENV-3 3'-UTR with that of DENV-4. *Vaccine*, **26**, 817–828.
26. Gritsun, T.S., Venugopal, K., Zlotoff, P.M., Mikhailov, M.V., Sall, A.A., Holmes, E.C., Polkinghorne, I., Frolova, T.V., Pogodina, V.V., Lashkevich, V.A. et al. (1997) Complete sequence of two tick-borne flaviviruses isolated from Siberia and the UK: analysis and significance of the 5' and 3'-UTRs. *Virus Res.*, **49**, 27–39.
27. Gritsun, T.S., Tuplin, A.K. and Gould, E.A. (2006) Origin, evolution and function of flavivirus RNA in untranslated and coding regions: implications for virus transmission. In Kalitzky, M. and Borowski, P. (eds), *Flaviviridae: Pathogenesis, Molecular Biology and Genetics*. Horizon Scientific Press, Norwich, UK, pp. 47–99.
28. Thurner, C., Witwer, C., Hofacker, I.L. and Stadler, P.F. (2004) Conserved RNA secondary structures in Flaviviridae genomes. *J. Gen. Virol.*, **85**, 1113–1124.
29. Thompson, J.D., Gibson, T.J., Jeanmougin, F. and Higgins, D.G. (1997) The ClustalX windows interface: flexible strategies for multiple sequence alignment aided by quality analysis tools. *Nucleic Acids Res.*, **25**, 4876–4882.
30. Simmonds, P., Tuplin, A. and Evans, D.J. (2004) Detection of genome-scale ordered RNA structure (GORS) in genomes of positive-stranded RNA viruses: Implications for virus evolution and host persistence. *RNA*, **10**, 1337–1351.
31. Zuker, M. (2003) Mfold web server for nucleic acid folding and hybridization prediction. *Nucleic Acids Res.*, **31**, 3406–3415.
32. Markham, N.R. and Zuker, M. (2005) DINAMelt web server for nucleic acid melting prediction. *Nucleic Acids Res.*, **33**, W577–581.
33. Gritsun, T.S., Frolova, T.V., Pogodina, V.V., Lashkevich, V.A., Venugopal, K. and Gould, E.A. (1993) Nucleotide and deduced amino acid sequence of the envelope gene of the Vasilchenko strain of TBE virus; comparison with other flaviviruses. *Virus Res.*, **27**, 201–209.
34. Gritsun, T.S. and Gould, E.A. (1998) Development and analysis of a tick-borne encephalitis virus infectious clone using a novel and rapid strategy. *J. Virol. Methods*, **76**, 109–120.
35. Gritsun, T.S. and Gould, E.A. (1995) Infectious transcripts of tick-borne encephalitis virus, generated in days by RT-PCR. *Virology*, **214**, 611–618.
36. Gritsun, T.S., Desai, A. and Gould, E.A. (2001) The degree of attenuation of tick-borne encephalitis virus depends on the cumulative effects of point mutations. *J. Gen. Virol.*, **82**, 1667–1675.
37. Grard, G., Moureau, G., Charrel, R.N., Lemasson, J.J., Gonzalez, J.P., Gallian, P., Gritsun, T.S., Holmes, E.C., Gould, E.A. and de Lamballerie, X. (2007) Genetic characterization of tick-borne flaviviruses: new insights into evolution, pathogenetic determinants and taxonomy. *Virology*, **361**, 80–92.
38. Mohan, S., Hsiao, C., Bowman, J.C., Wartell, R. and Williams, L.D. RNA tetraloop folding reveals tension between backbone restraints and molecular interactions. *J. Am. Chem. Soc.*, **132**, 12679–12689.
39. Antao, V.P. and Tinoco, I. Jr (1992) Thermodynamic parameters for loop formation in RNA and DNA hairpin tetraloops. *Nucleic Acids Res.*, **20**, 819–824.
40. Tuplin, A., Evans, D.J. and Simmonds, P. (2004) Detailed mapping of RNA secondary structures in core and NS5B-encoding region sequences of hepatitis C virus by RNase cleavage and novel bioinformatic prediction methods. *J. Gen. Virol.*, **85**, 3037–3047.
41. Barr, J.N. and Fearn, R. How RNA viruses maintain their genome integrity. *J. Gen. Virol.*, **91**, 1373–1387.
42. Kofler, R.M., Heinz, F.X. and Mandl, C.W. (2002) Capsid protein C of tick-borne encephalitis virus tolerates large internal deletions and is a favorable target for attenuation of virulence. *J. Virol.*, **76**, 3534–3543.
43. Gritsun, T.S. and Gould, E.A. (2007) Direct repeats in the flavivirus 3' untranslated region; a strategy for survival in the environment? *Virology*, **358**, 258–265.
44. Gritsun, T.S. and Gould, E.A. (2006) The 3' untranslated regions of Kamiti River virus and Cell fusing agent virus originated by self-duplication. *J. Gen. Virol.*, **87**, 2615–2619.
45. Schuppli, D., Miranda, G., Qiu, S. and Weber, H. (1998) A branched stem-loop structure in the M-site of bacteriophage Qbeta RNA is important for template recognition by Qbeta replicase holoenzyme. *J. Mol. Biol.*, **283**, 585–593.
46. Klovins, J., Berzins, V. and van Duin, J. (1998) A long-range interaction in Qbeta RNA that bridges the thousand nucleotides between the M-site and the 3' end is required for replication. *RNA*, **4**, 948–957.
47. McKnight, K.L. and Lemon, S.M. (1996) Capsid coding sequence is required for efficient replication of human rhinovirus 14 RNA. *J. Virol.*, **70**, 1941–1952.
48. Kim, Y.N. and Makino, S. (1995) Characterization of a murine coronavirus defective interfering RNA internal cis-acting replication signal. *J. Virol.*, **69**, 4963–4971.
49. Goodfellow, I.G., Kerrigan, D. and Evans, D.J. (2003) Structure and function analysis of the poliovirus cis-acting replication element (CRE). *RNA*, **9**, 124–137.
50. Gerber, K., Wimmer, E. and Paul, A.V. (2001) Biochemical and genetic studies of the initiation of human rhinovirus 2 RNA replication: identification of a cis-replicating element in the coding sequence of 2A(pro). *J. Virol.*, **75**, 10979–10990.
51. Goodfellow, I., Chaudhry, Y., Richardson, A., Meredith, J., Almond, J.W., Barclay, W. and Evans, D.J. (2000) Identification of

- a cis-acting replication element within the poliovirus coding region. *J. Virol.*, **74**, 4590–4600.
52. Rieder,E., Paul,A.V., Kim,D.W., van Boom,J.H. and Wimmer,E. (2000) Genetic and biochemical studies of poliovirus cis-acting replication element cre in relation to VPg uridylylation. *J. Virol.*, **74**, 10371–10380.
 53. Herold,J. and Andino,R. (2001) Poliovirus RNA replication requires genome circularization through a protein-protein bridge. *Mol. Cell*, **7**, 581–591.
 54. Sullivan,M.L. and Ahlquist,P. (1999) A brome mosaic virus intergenic RNA3 replication signal functions with viral replication protein 1a to dramatically stabilize RNA in vivo. *J. Virol.*, **73**, 2622–2632.
 55. Gamarnik,A.V. and Andino,R. (1998) Switch from translation to RNA replication in a positive-stranded RNA virus. *Gene. Dev.*, **12**, 2293–2304.
 56. Kanamori,H., Yuhashi,K., Ohnishi,S., Koike,K. and Kodama,T. (2010) RNA dependent RNA polymerase of hepatitis C virus binds to its coding region RNA stem-loop structure, 5BSL3.2, and its negative strand. *J. Gen. Virol.*, **91**, 1207–1212.
 57. Villordo,S.M., Alvarez,D.E. and Gamarnik,A.V. (2010) A balance between circular and linear forms of the dengue virus genome is crucial for viral replication. *RNA*, **16**, 2325–2335.
 58. Mir,M.A. and Panganiban,A.T. (2006) The bunyavirus nucleocapsid protein is an RNA chaperone: possible roles in viral RNA panhandle formation and genome replication. *RNA*, **12**, 272–282.
 59. Gould,E.A., de Lamballerie,X., Zanotto,P.M. and Holmes,E.C. (2003) Origins, evolution, and vector/host coadaptations within the genus Flavivirus. *Adv. Virus Res.*, **59**, 277–314.
 60. Labuda,M., Austyn,J.M., Zuffova,E., Kozuch,O., Fuchsberger,N., Lysy,J. and Nuttall,P.A. (1996) Importance of localized skin infection in tick-borne encephalitis virus transmission. *Virology*, **219**, 357–366.
 61. Khasnatinov,M.A., Ustanikova,K., Frolova,T.V., Pogodina,V.V., Bochkova,N.G., Levina,L.S., Slovak,M., Kazimirova,M., Labuda,M., Klempa,B. *et al.* (2009) Non-hemagglutinating flaviviruses: molecular mechanisms for the emergence of new strains via adaptation to European ticks. *PLoS One*, **4**, e7295.